Gain-Driven Discrete Breathers in $\mathcal{PT}-$Symmetric Nonlinear Metamaterials

N. Lazarides[1,2], G. P. Tsironis[1,2]
[1] *Department of Physics, University of Crete, P. O. Box 2208, 71003 Heraklion, Greece;*
[2] *Institute of Electronic Structure and Laser, Foundation for Research and Technology-Hellas, P.O. Box 1527, 71110 Heraklion, Greece*

(Dated: May 3, 2014)

We introduce a one dimensional parity-time ($\mathcal{PT}$)-symmetric nonlinear magnetic metamaterial consisting of split-ring dimers having both gain and loss. When nonlinearity is absent we find a transition between an exact to a broken $\mathcal{PT}$-phase; in the former the system features a two band gapped spectrum with shape determined by the gain and loss coefficients as well as the inter-unit coupling. In the presence of nonlinearity we show numerically that as a result of the gain/dissipation matching a novel type of long-lived stable discrete breathers can form below the lower branch of the band with no attenuation. In these localized modes the energy is almost equally partitioned between two adjacent split rings on the one with gain and the other one with loss.

PACS numbers: 63.20.Pw, 11.30.Er, 41.20.-q, 78.67.Pt

Considerable research effort has recently focused in the investigation and developement of artificial materials that exhibit properties not found in nature. In the electromagnetic domain, these advances resulted in the construction of metamaterials, novel artificial structures that provide full access to all four quadrants of the real permittivity - permeability plane [1]. Recently, there has been increasing interest in synthetic materials with a combined parity - time ($\mathcal{PT}$) symmetry. Although quantum systems described by $\mathcal{PT}-$symmetric Hamiltonians have been studied for many years ([2] and refs. therein), it was only recently realized that many classical systems are $\mathcal{PT}-$symmetric [3]. Subsequently, the notion of $\mathcal{PT}$ symmetry has been extended to dynamical lattices, particularly in optics [4, 5]. Soon after that, $\mathcal{PT}-$symmetry breaking was experimentally observed [6–8]. Such considerations have been also extended in nonlinear lattices, where the existence of stable discrete solitons [9] and Talbot effects [10] was theoretically demonstrated.

Among recent developements in $\mathcal{PT}-$symmetric materials, the application of these ideas in electronic circuits [11] not only provides a platform for testing the new ideas within the framework of easily accessible experimental configurations, but also provides a link to metamaterials. Conventional, metallic metamaterials suffer from high losses that hamper their use in practical applications. However, building metamaterials with $\mathcal{PT}$ symmetry, relying on gain and loss, may provide a way out and moreover lead to new extraordinary properties. It is shown that $\mathcal{PT}-$symmetric metamaterials undergo spontaneous symmetry breaking from the exact $\mathcal{PT}$ phase (real eigenfrequencies) to the broken $\mathcal{PT}$ phase (at least a pair of complex eigenfrequencies), with variation of the gain/loss coefficient. In the presence of nonlinearity, the generation of long-lived excitations in the form of discrete breathers (DBs) [12] is demonstrated numerically in metamaterial models. These novel gain-driven DBs, generated either by proper intialization of the $\mathcal{PT}$ metamaterial or purely dynamically through external driving, result from power matching of the input power through the gain mechanism and internal loss.

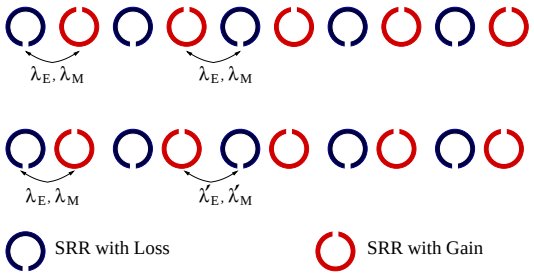

FIG. 1: (Color online) Schematic of a $\mathcal{PT}$ metamaterial. Upper panel: all the SRRs are equidistant. Lower panel: the separation between SRRs is modulated according to a binary pattern ($\mathcal{PT}$ dimer chain).

Consider a one-dimensional array of dimers, each comprising two nonlinear split-ring resonators (SRRs); one with loss and the other with equal amount of gain (Fig. 1). The SRRs are coupled magnetically and/or electrically through dipole-dipole forces [13–16] and are regarded as RLC circuits, featuring a resistance R, an inductance L, and a capacitance C. Early realizations of nonlinear metamaterial elements employed a varicap diode [17]; subsequently several types of diodes have been employed to demonstrate single tunable elements [18, 19] and metamaterials [20]. For constructing active metamaterials, the incorporation of constituents that provide gain through external energy sources is a promising technique [21]. In particular realizations, a tunnel (Esaki) diode [22] featuring negative resistance has been employed [23]. Low-loss, active metamaterials have been demonstrated as left-handed transmission lines [23] and optical fishnet structures [24]. However, there are still open issues concerning gain operation in metamaterials, related to noise and other effects that come into play [25].

In the equivalent circuit model picture [16, 26–28], ex-

tended for the $\mathcal{PT}$ dimer chain, the dynamics of the charge q_n in the capacitor of the nth SRR is governed by

$$\begin{aligned} \lambda'_M \ddot{q}_{2n} &+ \ddot{q}_{2n+1} + \lambda_M \ddot{q}_{2n+2} + \lambda'_E q_{2n} + q_{2n+1} + \lambda_E q_{2n+2} \\ &= \varepsilon_0 \sin(\Omega\tau) - \alpha q_{2n+1}^2 - \beta q_{2n+1}^3 - \gamma \dot{q}_{2n+1} \quad (1) \\ \lambda_M \ddot{q}_{2n-1} &+ \ddot{q}_{2n} + \lambda'_M \ddot{q}_{2n+1} + \lambda_E q_{2n-1} + q_{2n} + \lambda'_E q_{2n+1} \\ &= \varepsilon_0 \sin(\Omega\tau) - \alpha q_{2n}^2 - \beta q_{2n}^3 + \gamma \dot{q}_{2n} \quad (2) \end{aligned}$$

where λ_M, λ'_M and λ_E, λ'_E are the magnetic and electric interaction coefficients, respectively, between nearest neighbors, α and β are nonlinear coefficients, γ is the gain/loss coefficient ($\gamma > 0$), ε_0 is the amplitude of the external driving voltage, while Ω and τ are the driving frequency and temporal variable, respectively, normalized to $\omega_0 = 1/\sqrt{LC_0}$ and ω_0^{-1}, respectively, with C_0 being the linear capacitance. We have also considered additional next-nearest neighbor coupling between SRRs, with coefficients that fall off as the inverse-cube of the distance between them. Although slight quantitative changes are observed, the results presented below are not qualitatively affected. The chosen values of the nonlinearity coefficients are typical for a diode [28], while γ chosen to provide stable operation. The coupling coefficients are chosen relatively large for clarity. However, breathers appear generically even for weakly coupled SRRs.

By substituting $q_{2n} = A\exp[i(2n\kappa - \Omega\tau)]$ and $q_{2n+1} = B\exp[i((2n+1)\kappa - \Omega\tau)]$, where κ is the normalized wavevector, into Eqs. (1) and (2), and requesting nontrivial solutions for the resulting stationary problem, we obtain

$$\Omega_\kappa^2 = \left(-b \pm \sqrt{\Delta}\right)/(2a), \quad (3)$$

where $a = 1 - (\lambda_M - \lambda'_M)^2 - \mu_\kappa \mu'_\kappa$, $b = \gamma^2 - 2\left[1 - (\lambda_E - \lambda'_E)(\lambda_M - \lambda'_M)\right] + \varepsilon_\kappa \mu'_\kappa + \varepsilon'_\kappa \mu_\kappa$, $c = 1 - (\lambda_E - \lambda'_E)^2 - \varepsilon_\kappa \varepsilon'_\kappa$, $\Delta = b^2 - 4ac$, and $\varepsilon_\kappa = 2\lambda_E \cos(\kappa)$, $\varepsilon'_\kappa = 2\lambda'_E \cos(\kappa)$, $\mu_\kappa = 2\lambda_M \cos(\kappa)$, $\mu'_\kappa = 2\lambda'_M \cos(\kappa)$. In the following, we consider that the relative orientation of the SRRs in the chain is such that the magnetic coupling dominates, while the electric coupling can be neglected (Fig. 1) [14]. Then, Eq. (3) reduces to

$$\Omega_\kappa^2 = \frac{2 - \gamma^2 \pm \sqrt{\gamma^4 - 2\gamma^2 + (\lambda_M - \lambda'_M)^2 + \mu_\kappa \mu'_\kappa}}{2(1 - (\lambda_M - \lambda'_M)^2 - \mu_\kappa \mu'_\kappa)}. \quad (4)$$

The condition for Ω_κ being real for any κ then reads

$$\cos^2(\kappa) \geq \frac{\gamma^2(2 - \gamma^2) - (\lambda_M - \lambda'_M)^2}{4\lambda_M \lambda'_M}. \quad (5)$$

For $\lambda_M = \lambda'_M$ Eq. (5) cannot be satisfied for all κ's for any $\gamma > 0$, implying that a large $\mathcal{PT}-$symmetric SRR array (Fig. 1, upper) is in the broken phase. However, for a dimer chain with $\lambda_M \neq \lambda'_M$ (Fig. 1, lower), the above condition is satisfied for all κ's for $\gamma \leq \gamma_c \simeq |\lambda_M - \lambda'_M|$, ($\gamma^4 \simeq 0$). In the exact phase ($\gamma < \gamma_c$), the $\mathcal{PT}$ dimer chain has a gapped spectrum with two frequency bands [Fig 2(a)]. The width of the gap separating the bands decreases with decreasing $|\lambda_M - \lambda'_M|$ for constant γ. For $\gamma \simeq \gamma_c$ the gap closes [Fig. 2(b)], some frequencies in the spectrum acquire imaginary parts [Fig. 2(c)] and $\mathcal{PT}-$symmetry breaking occurs. A typical phase diagram on the $\gamma - r_M$ plane, with $r_M = \lambda'_M/\lambda_M$, is shown in Fig. 2(d). The solid lines indicate the variation of the exceptional point γ_c that separates the exact from the broken phase. For fixed λ_M, λ'_M, the bandwidths as a function of γ are shown in Fig. 3.

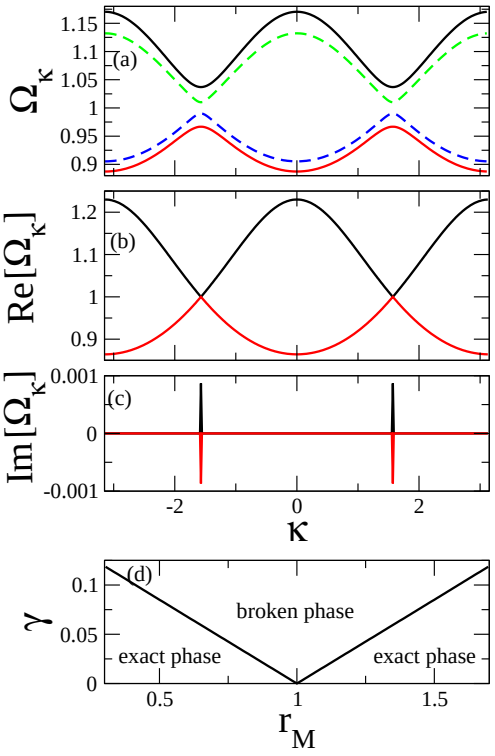

FIG. 2: (Color online) (a) Frequency bands for a $\mathcal{PT}$ metamaterial for $\gamma = 0.002$, and $\lambda_M = -0.17$, $\lambda'_M = -0.10$ (black and red solid lines); $\lambda_M = -0.12$, $\lambda'_M = -0.10$ (green and blue dashed lines). The imaginary parts are zero. (b) & (c) Real and imaginary parts, respectively, of the frequency bands for a $\mathcal{PT}$ metamaterial with $\gamma = 0.002$, $\lambda_M = -0.17$, $\lambda'_M = -0.1699$. (d) $\mathcal{PT}$ phase diagram on the $\gamma - r_M$ plane ($r_M = \lambda'_M/\lambda_M$), for $\lambda_M = -0.17$.

Eqs. (1) and (2), implemented with $q_0(\tau) = q_{N+1}(\tau) = 0$, are integrated numerically with $q_m(0) = (-1)^{m-1}\mathrm{sech}(m/2)$, $\dot{q}_m(0) = 0$, and $\varepsilon_0 = 0$, $\alpha = -0.4$, $\beta = 0.08$. Using a gain/loss function of the form

$$\gamma(m) = \begin{cases} \gamma, & m = 1, ..., N_\ell \\ (-1)^{m-1}\gamma, & m = N_\ell + 1, ..., N - N_\ell \\ \gamma, & m = N - N_\ell + 1, ..., N, \end{cases} \quad (6)$$

we obtain gain-driven, long-lived ($> 10^8$ time units) DBs for wide parameter intervals. Note that the actual $\mathcal{PT}$ dimer chain is of length $N - 2N_\ell$, while both its ends

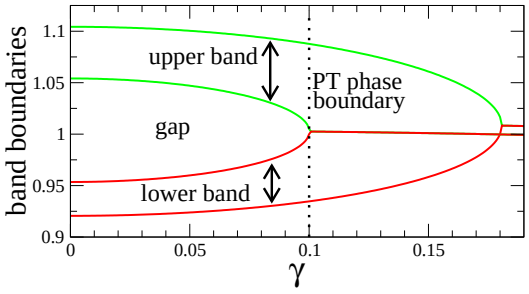

FIG. 3: (Color online) Frequency band boundaries as a function of γ for a $\mathcal{PT}$ dimer chain with $\lambda_M = -0.14$, $\lambda'_M = -0.04$.

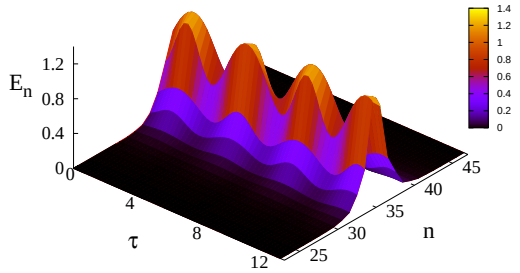

FIG. 4: (Color online) Spatiotemporal evolution of the energy density E_n during two periods for $N = 70$, $N_\ell = 10$, $\lambda'_M = -0.10$, $\lambda_E = \lambda'_E = 0$, $\gamma = 0.002$, and $\lambda_M = -0.17$.

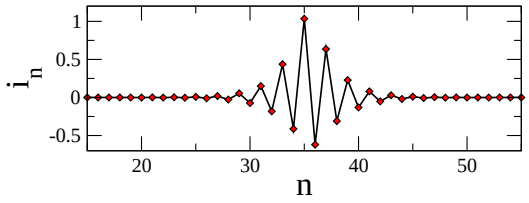

FIG. 5: (Color online) Gain-driven, current breather profile i_n as a function of n, for $N = 70$, $N_\ell = 10$, $\lambda'_M = -0.10$, $\lambda_E = \lambda'_E = 0$, $\gamma = 0.002$, and $\lambda_M = -0.17$.

are joined to lossy dimer chains of length N_ℓ. We found empirically that this is the most effective way to stabilize DBs in the $\mathcal{PT}$ metamaterial, i.e., by embedding it into a lossy metamaterial. The lossy parts help the excess energy to go smothly away during the long transient phase of integration, and thus prevents the blowing up of the solution that otherwise may have occured. The energy density E_n evolution of a typical DB in the $n - \tau$ plane is shown in Fig. 4. The largest part of the total energy is concentrated into two neighboring sites belonging to the same dimer. The corresponding instantaneous current profile i_n at maximum current (Fig. 5) is neither symmetric or antisymmetric at the single SRR level.

The breather frequency Ω_B can be obtained from the

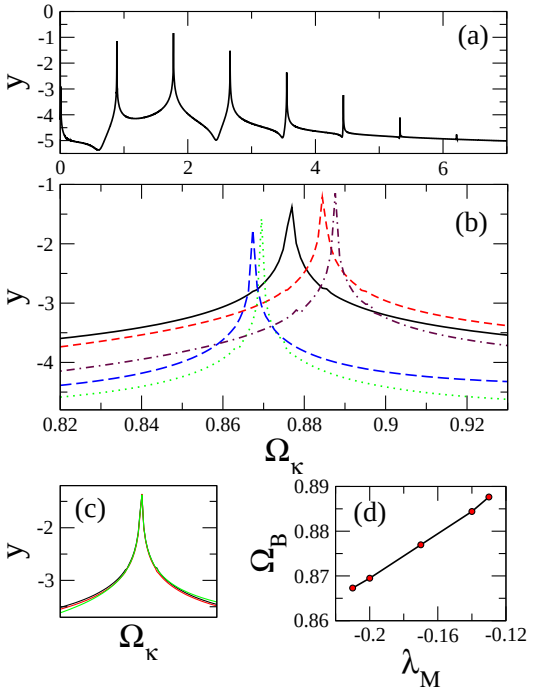

FIG. 6: (Color online) (a) The logarithm of the power spectrum of energy at one of the central breather sites $y = log_{10}[PS(E_{n=N/2})]$ as a function of Ω_κ, for $N = 70$, $\lambda'_M = -0.10$, $\lambda_M = -0.13$, $\lambda_E = \lambda'_E = 0$, $\gamma = 0.002$. (b) The same as in (a) around the fundamental breather frequency Ω_B, for $\lambda_M = -0.21$ (blue - long dashed); $\lambda_M = -0.20$ (green - dotted); $\lambda_M = -0.17$ (black - solid); $\lambda_M = -0.14$ (red - dashed); $\lambda_M = -0.13$ (maroon - dotted dashed). The other parameters as in (a). (c) The same as in (a) and (b) around Ω_B, for $\gamma = 0.002$ (black); 0.005 (green); 0.01 (red). (d) Dependence of Ω_B on λ_M for the spectra in (b).

power spectrum of a time series of the energy in one of the DB sites. The logarithm of a typical power spectrum is plotted as a function of frequency in Fig. 6(a); strong harmonics to the fundamental frequency Ω_B are observed. The frequency Ω_B increases with decreasing $|\lambda_M - \lambda'_M|$ [Fig. 6(b)], while the variation of γ within $10^{-2} - 10^{-3}$ has apparently no effect on Ω_B at least in the particular case shown in Fig. 6(c). The dependence of Ω_B on $|\lambda_M - \lambda'_M|$ is illustrated in Fig. 6(d), for those values of $|\lambda_M - \lambda'_M|$ for which DBs are stable (or at least long-lived).

For a gapped linear spectrum, large amplitude linear modes become unstable in the presence of driving and nonlinearity. If the curvature of the dispersion curve in the region of such a mode is positive and the lattice potential is soft, large amplitude modes become unstable with respect to DB formation in the gap below the linear spectrum [29]. For the parameters of Fig. 2(a), the bottom of the lower band is located at $\Omega_0 \simeq 0.887$, where the curvature is positive. Moreover, the SRRs are subjected to soft on-site potentials for the selected values of α and β. Then, DBs can be generated spontaneously by

a frequency chirped driver as it is illustrated in Fig. 7, where the energy density E_n for a $\mathcal{PT}$ dimer chain is plotted on the $n-\tau$ plane. We use the following procedure: At time $\tau = 0$, we start integrating Eqs. (1) and (2) with zero initial state and external driving for 500 $T_0 \simeq 3500$ time units (t.u.), where $T_0 = 2\pi/\Omega_0$, to allow for significant developement of large amplitude modes. At time $\tau \simeq 3500$ t.u. (point A on Fig. 7), the driver is switched-on with low-amplitude and frequency slightly above Ω_0 ($1.01\ \Omega_0 \simeq 0.894$). The frequency is then chirped downwards with time to induce instability for the next $10,600$ t.u. ($\sim 1500\ T_0$), until it is well below Ω_0 ($0.997\ \Omega_0 \simeq 0.882$). During that phase, a large number of excitations are generated that move and strongly interact to each other, eventually merging into a small number of high amplitude (multi-)breathers. At time $\tau \simeq 14,100$ t.u. (point B on Fig. 7), the driver is switched off and the DBs that have formed are solely driven by the gain. They continue to interact until they reach a stationary state and get trapped at particular sites. The high density segments between points B and C in Fig. 7 present precisely those stationary gain-driven (multi-)breathers generated through chirping and subsequent dynamics. At time $\tau \sim 85150$ t.u. (point C on Fig. 7), the gain is replaced by equal amount of loss, and the breathers die out rapidly.

The construction of a $\mathcal{PT}$ metamaterial is feasible with the present technology in the microwaves, where negative resistance devices [23, 30] and transistors [31] are convenient for providing gain. Thus, $\mathcal{PT}$ dimers can be constructed and balanced in a way similar to that in electrical circuits [11]. For SRR dimers, highly conducting rings are required for reduced Ohmic losses. The bias of the negative resistance device in the SRR with gain should be adjusted to provide a gain coefficient with magnitude equal to that of the loss coefficient of the SRR without gain. A chain of such dimers makes a $\mathcal{PT}$ metamaterial whose dynamics is approximatelly described by model Eqs. (1) and (2).

For a balanced configuration the metamaterial exhibits two bands separated by a gap. While the band structure appears to be stable to small structural perturbations, it may be more fragile in the case of relatively strong disorder [32, 33]. However, any divergence related to a disorder-induced broken phase will manifest itself in time-scales larger than the characteristic interdimer dynamics time-scale, making possible the experimental observation in real $\mathcal{PT}$ systems (e.g. in Ref. [11]).

It is demonstrated numerically that stable or at least long-lived, gain-driven DBs may be excited generically. DBs result either by proper initialization of the system, or purely dynamically by frequency chirping of a weak alternating driver. Fundamental DBs occupy two neighboring sites that belong to the same dimer. Stability and long life-times of DBs is achieved by embedding the $\mathcal{PT}-$symmetric dimer chain into a lossy dimer chain.

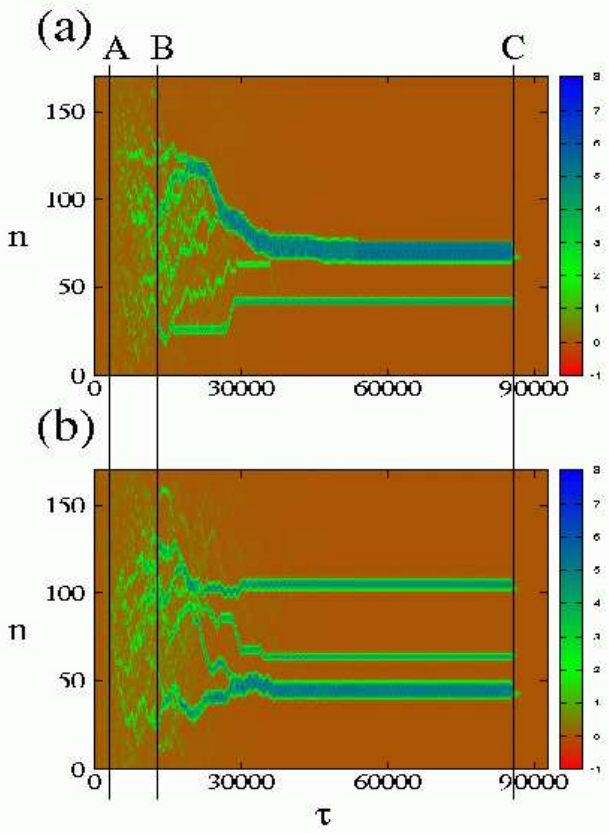

FIG. 7: (Color online) The energy density E_n on the $n-\tau$ plane for a $\mathcal{PT}$ dimer chain with $N = 170$, $N_\ell = 10$, $\Omega_0 = 0.887$, $\gamma = 0.002$, $\lambda_M = -0.17$, $\lambda'_M = -0.10$ ($\lambda_E = \lambda'_E = 0$), and (a) $\varepsilon_0 = 0.085$; (b) $\varepsilon_0 = 0.095$. The vertical lines separate different stages in the chirping procedure.

When the balance between gain and loss is not exact, i.e., when the magnitudes of the gain and loss coefficients differ by a small amount, DBs can still be generated through the chirping procedure. In this case, however, the DBs lose their long-term stability, viz. for loss exceeding gain they decay slowly until they vanish while in the opposite case the DBs gain energy and diverge. Both effects occur on a time-scale related to the gain-loss imbalance.

This work was supported by the "THALES" Project ANEMOS, funded by the ESPA Program of the Ministry of Education of Greece.

[1] N. I. Zheludev, Science **328**, 582 (2010), and refs therein.
[2] D. W. Hook, Ann. Phys. (Berlin) **524**, A106 (2012).
[3] C. M. Bender, D. D. Holm, and D. W. Hook, J. Phys. A: Math. Theor. **40**, F793 (2007).
[4] R. El-Ganainy *et al.*, Opt. Lett. **32**, 2632 (2007).
[5] K. G. Makris *et al.*, Phys. Rev. Lett. **100**, 103904 (2008).
[6] A. Guo *et al.*, Phys. Rev. Lett. **103**, 093902 (2009).
[7] C. E. Rüter *et al.*, Nature Physics **6**, 192 (2010).

[8] A. Szameit *et al.*, Phys. Rev. **A 84**, 021806(R) (2011).
[9] S. V. Dmitriev, A. A. Sukhorukov, and Yu. S. Kivshar, Opt. Lett. **35**, 2976 (2010).
[10] H. Ramezani *et al.*, Phys. Rev. Lett. **109**, 033902 (2012).
[11] J. Schindler *et al.*, Phys. Rev. A **84**, 040101(R) (2011).
[12] S. Flach and A. V. Gorbach, Phys. Rep. **467**, 1 (2008).
[13] O. Sydoruk *et al.*, Phys. Rev. B **73**, 224406 (2006).
[14] F. Hesmer *et al.*, Phys. Stat. Sol. (B) **244**, 1170 (2007).
[15] I. Sersić *et al.*, Phys. Rev. Lett. **103**, 213902 (2009).
[16] N. N. Rosanov *et al.*, Opt. Express **19**, 26500 (2011).
[17] O. Reynet and O. Acher, Appl. Phys. Lett. **84**, 1198 (2004).
[18] D. A. Powell *et al.*, Appl. Phys. Lett. **91**, 144107 (2007).
[19] B. Wang *et al.*, Opt. Express **16**, 16058 (2008).
[20] I. V. Shadrivov *et al.*, Appl. Phys. Lett. **93**, 161903 (2008).
[21] A. D. Boardman *et al.*, Laser Photonics Rev. **5**, 287 (2010).
[22] L. Esaki, Phys. Rev. **109**, 603 (1958).
[23] T. Jiang *et al.*, Phys. Rev. Lett. **107**, 205503 (2011).
[24] S. Xiao *et al.*, Nature **466**, 735 (2010).
[25] R. R. A. Syms and L. Solymar, J. Appl. Phys. **109**, 124909 (2011).
[26] N. Lazarides, M. Eleftheriou, and G. P. Tsironis, Phys. Rev. Lett. **97**, 157406 (2006).
[27] M. I. Molina, N. Lazarides, and G. P. Tsironis, Phys. Rev. E **80**, 046605 (2009).
[28] N. Lazarides, V. Paltoglou, and G. P. Tsironis, Int. J. Bifurcation Chaos **21**, 2147 (2011).
[29] M. Sato *et al.*, Phys. Rev. Lett. **90**, 044102 (2003).
[30] A. D. Boardman *et al.*, J. Opt. Soc. Am. B **24**, A53-A61 (2007).
[31] W. Xu, W. J. Padilla, and S. Sonkusale, arXiv:1204.6067
[32] O. Bendix, R. Fleischmann, T. Kottos, and B. Shapiro, Phys. Rev. Lett. **103**, 030402 (2009).
[33] N. Lazarides and G. P. Tsironis, work in progress (2012).